Russian Geology and Geophysics © 2020, V.S. Sobolev IGM, Siberian Branch of the RAS
Vol. 61, No. 5–6, pp. 650–662, 2020 *DOI:10.15372/RGG2020115* *Geologiya i Geofizika*

Experimental Modeling of Decarbonation Reactions Resulting in Mg,Fe-garnets and CO_2 fluid at the Mantle *P–T* parameters

Yu.V. Bataleva[a, ✉], I.D. Novoselov[a,b], A.N. Kruk[a], O.V. Furman[a,b], V.N. Reutsky[a], Yu.N. Palyanov[a,b]

[a] *V.S. Sobolev Institute of Geology and Mineralogy, Siberian Branch of the Russian Academy of Sciences, pr. Akademika Koptyuga 3, Novosibirsk, 630090, Russia*

[b] *Novosibirsk State University, ul. Pirogova 1, Novosibirsk, 630090, Russia*

Received 22 January 2020; accepted 28 February 2020

Abstract—Experimental modeling of decarbonation reactions with the formation of Mg,Fe-garnets and CO_2 fluid during mantle–crust interactions was carried out in a wide range of the upper-mantle pressures and temperatures. Experimental studies were performed in the $MgCO_3$–Al_2O_3–SiO_2 and (Mg,Fe)CO_3–Al_2O_3–SiO_2 systems in the pressure range 3.0–7.5 GPa and temperature range 950–1450 °C (t = 10–60 h), using a multianvil high-pressure apparatus of the "split-sphere" type (BARS). Experiments were carried out with a specially designed high-pressure buffered cell with a hematite container that prevents the diffusion of hydrogen into a Pt-capsule with a sample. It has been experimentally established that in the $MgCO_3$–Al_2O_3–SiO_2 system decarbonation occurs by the schematic reaction $MgCO_3 + SiO_2 + Al_2O_3 \rightarrow Mg_3Al_2Si_3O_{12} + CO_2$ at 1100 ± 20 °C (3.0 GPa), 1150 ± 20 °C (6.3 GPa), and 1400 ± 20 °C (7.5 GPa) and in the (Mg,Fe)CO_3–Al_2O_3–SiO_2 system, by the reaction (Mg,Fe)$CO_3 + SiO_2 + Al_2O_3 \rightarrow$ (Mg,Fe)$3Al_2Si_3O_{12} + CO_2$ at 1000 ± 20 °C (3.0 GPa), 1150 ± 20 °C (6.3 GPa), and 1400 ± 20 °C (7.5 GPa). Based on Raman spectroscopic characterization of the synthesized garnets, the position of the main modes R, υ_2, and υ_1 in the pyrope has been determined to be 364, 562, and 924–925 cm^{-1}, respectively, and that in pyrope-almandine, 350–351, 556–558, and 918–919 cm^{-1}. The effectiveness of the hematite container was demonstrated by means of mass spectrometry analysis. It has been found that the fluid composition corresponded to pure CO_2 in all experiments. The *P,T*-positions of decarbonation curves leading to the formation of a CO_2 fluid in assemblage with pyrope and pyrope-almandine have been experimentally reconstructed and compared with the previous calculation and experimental data. It has been established that the experimentally reproduced reaction lines with the formation of pyrope + CO_2 or pyrope-almandine + CO_2 assemblages are shifted to lower temperatures by 50–150 °C relative to the calculated ones. When considering the obtained results with regard to the stability of natural carbonates of various compositions in subduction settings, it has been found that at depths of ~90–190 km Mg,Fe-carbonates react with oxides in the temperature range 1000–1250 °C, and at depths of ~225 km, at 1400 °C.

Keywords: decarbonation, CO_2 fluid, mantle carbonates, garnet, high-pressure experiment, experimental modeling

INTRODUCTION

Studies of natural carbonates stability conditions and features of the CO_2 fluid generation during mantle-crust interaction are critical for the reconstruction of global carbon cycle processes, including mantle metasomatism, natural diamond formation, and the formation and evolution of carbonated eclogites and peridotites (Luth, 1999; Shirey et al., 2013; Plank and Manning, 2019; Stagno et al., 2019). To date, it has been established that carbonates can be subducted to depths of more than 600 km (Shirey et al., 2013), while they are thermodynamically stable at the *P–T* parameters of the lower mantle (Oganov et al., 2013). A direct evidence of the presence of carbonates in mantle rocks is their numerous findings in inclusions in diamonds (Navon et al., 1988; Schrauder and Navon, 1994; Bulanova, 1995; Wang et al., 1996; Sobolev et al., 1997; Stachel et al., 1998; Izraeli et al., 2001; Brenker et al., 2007; Kaminsky et al., 2013).

✉ Corresponding author.
E-mail address: bataleva@igm.nsc.ru (Yu.V. Bataleva)

The key factors determining the stability of carbonates in the mantle are pressure, temperature, oxygen fugacity and environmental composition. Their variations can lead to phase transitions and changes in the structure of carbonates (Luth, 1999; Stagno et al., 2019), initiate partial melting processes (Fig. 1) (Dasgupta and Hirschmann, 2010; Jones et al., 2013; Shatskiy et al., 2015), decomposition (break down) of carbonates (Morlidge et al., 2006; Jones et al., 2013; Shatskiy et al., 2015) or various carbonate-consuming reactions. The latter include diamond-forming redox reactions between carbonates and highly reduced phases (metallic iron, carbides, sulfides, reduced fluids and melts) (Gunn and Luth, 2006; Palyanov et al., 2007, 2013; Bataleva et al., 2016) and decarbonation reactions occurring during the interaction of carbonates with silicates and/or oxides, which lead to the formation of a CO_2 fluid and crystallization of newly formed silicates.

Decarbonation is one of the most common fluid-generating processes that occur during the interaction of the material of a subducting slab with mantle oxides or silicates, and determine the stability of carbonates in carbonate-oxide or

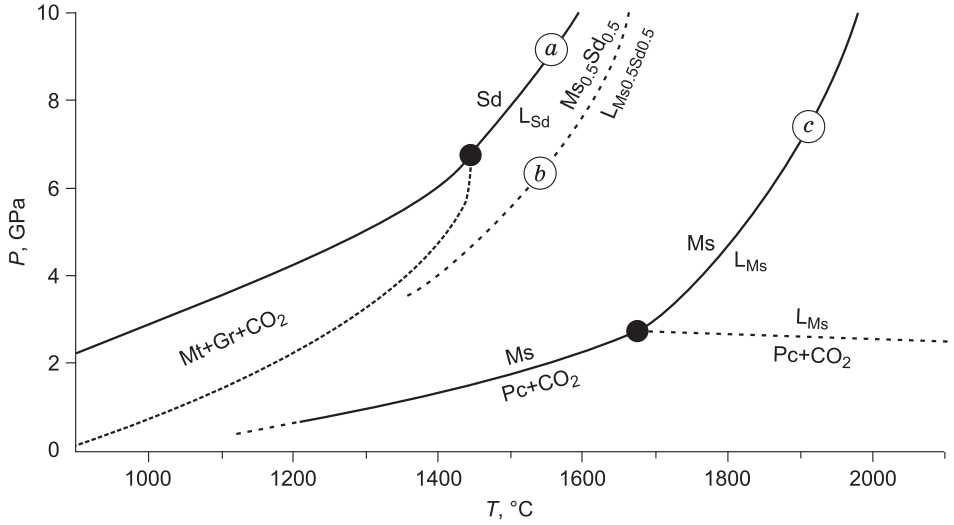

Fig. 1. Experimentally determined *P–T* parameters of melting and decomposition of magnesian-ferrous carbonates, according to Kang et al. (2015) and Tao et al. (2013) (*a,* siderite); Kang et al. (2016) (*b*, siderite-magnesite solid solution); Katsuro and Ito, (1990) (*c*, magnesite). Sd, siderite; L_{Sd}, liquid $FeCO_3$; Mt, magnetite; Gr, graphite; Ms, magnesite; Per, periclase; L_{Ms}, liquid $MgCO_3$; $Ms_{0.5}Sd_{0.5}$, siderite magnesite solid solution in the ratio 50/50; $L_{Ms0.5Sd0.5}$, $Mg_{0.5}Fe_{0.5}CO_3$ melt.

carbonate-silicate media. Depending on the composition of carbonates, as well as the host rocks, the *P–T* parameters of decarbonation can vary in a very wide range. For example, subducted $MgCO_3$ and $CaCO_3$ can be thermodynamically stable to the depths of the lower mantle (Brenker et al., 2007; Boulard et al., 2011; Merlini et al., 2012; Oganov et al., 2013), while the introduction of iron or manganese impurities in carbonates, as well as the presence of oxide minerals in the host rocks, can reduce the temperature of the onset of decarbonation reactions by several hundred degrees and 1-2 GPa (Berman, 1991; Martin and Hammouda, 2011). In addition to the generation of CO_2 fluid, the implementation of decarbonation reactions in the mantle wedge/slab interaction zones leads to the formation of various mantle silicates – olivine, pyroxenes and garnet, which compositions depend on the chemical characteristics of the subducted carbonates and host rocks involved in the reaction.

In the majority of published experimental works, the modeling of decarbonation reactions was carried out in carbonate-oxide and carbonate-silicate systems, with the formation of forsterite, diopside, enstatite, as well as the forsterite + diopside assemblage (Fig. 2):

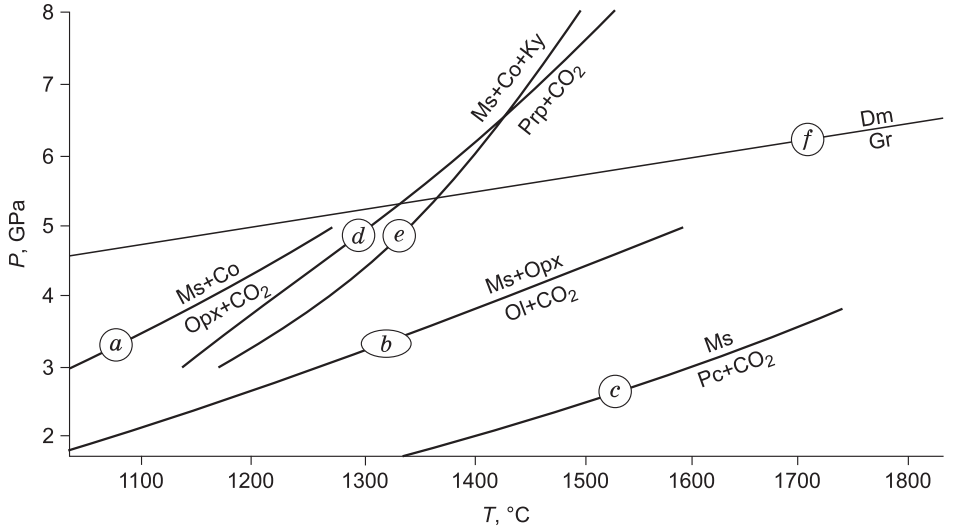

Fig. 2. *P–T* diagram with experimentally determined decarbonation reactions associated with the formation of CO_2-fluid and *a*, Orthopyroxene (Wyllie, 1979; Eggler, 1978; Wyllie et al., 1983; Pal'yanov et al., 2005); *b*, olivine (Newton and Sharp, 1975; Koziol and Newton, 1998); *c,* periclase (Shatsky et al., 2015) and *d*, garnet (Knoche et al., 1999), as well as the calculated position of the reaction Ms + Co + Ky = Prp + CO_2 (Knoche et al., 1999) (*e*). The graphite-diamond direct transition line (*f*) is given according to Kennedy and Kennedy (1976). Ms, magnesite; Pc, periclase; Opx, orthopyroxene (enstatite); Ol, olivine (forsterite); Co, coesite; Ky, kyanite; Prp, pyrope; Dm, diamond; Gr, graphite.

$MgSiO_3 + MgCO_3 \leftrightarrow Mg_2SiO_4 + CO_2$
(Newton and Sharp, 1975; Koziol and Newton, 1998); (1)

$MgCO_3 + SiO_2 \leftrightarrow MgSiO_3 + CO_2$ (Wyllie et al., 1983; Pal'yanov et al., 2005); (2)

$CaMg(CO_3)_2 + 2SiO_2 \leftrightarrow CaMgSi_2O_6 + 2CO_2$
(Luth, 1995); (3)

$(CaMg(CO_3)_2 + 4MgSiO_3 \leftrightarrow 2Mg_2SiO_4 + CaMgSi_2O_6 + 2CO_2$ (Wyllie, 1979; Eggler, 1978). (4)

However, experimental studies in carbonate-oxide and carbonate-silicate systems aimed at determining the formation parameters of the garnet + CO_2 assemblage under mantle *P–T* parameters are still scarce, only decarbonation parameters of MgO–Al_2O_3–SiO_2–CO_2 system were experimentally determined, with the formation of pyrope by following reactions:

$3MgCO_3 + Al_2SiO_5 + 2SiO_2 \leftrightarrow Mg_3Al_2Si_3O_{12} + 3CO_2$
(Knoche et al., 1999); (5)

$3MgCO_3 + Al_2O_3 + 3SiO_2 \leftrightarrow Mg_3Al_2Si_3O_{12} + 3CO_2$
(Pal'yanov et al., 2002, 2005). (6)

Moreover, the decarbonation reactions with the formation of ferrous or magnesian-ferrous silicates have not been studied experimentally, but their theoretical position was calculated in (Berman, 1991; Ogasawara et al., 1997). Thus, it seems relevant to determine the *P–T* regions of the stability of natural Mg,Fe-carbonates in assemblage with oxides, to perform experimental modeling of decarbonation reactions associated with the formation of garnets characteristic of mantle assemblages (pyrope and pyrope-almandine) and the formation of CO_2 fluid, and to determine the position of the corresponding decarbonation curves in a wide range of pressures and temperatures of the upper mantle as well.

METHODS

High-pressure, high-temperature experiments. Experimental modeling of decarbonation reactions resulting in the formation of Mg,Fe-garnets and CO_2 fluid was performed in $MgCO_3$–SiO_2–Al_2O_3 and (Mg,Fe)CO_3–SiO_2–Al_2O_3 systems using a split-sphere multi-anvil high-pressure apparatus (BARS) (Palyanov et al., 2010, 2017), at pressures of 3.0, 6.3 and 7.5 GPa, in the temperature range of 950–1450 °C and durations from 10 to 60 hours. Starting materials were natural carbonates – magnesite $Mg_{0.93}Ca_{0.06}Fe_{0.01}CO_3$ (Satka, Chelyabinsk Region, Russia) and magnesiosiderite $Fe_{0.6}Mg_{0.37}Ca_{0.02}Mn_{0.01}CO_3$ (Saint Pierre de Mazaj, France) (Fig. 3), as well as synthetic oxides – SiO_2 and Al_2O_3 (99.99% purity). Before experiments, starting materials were powdered, thoroughly mixed and then dried at a temperature of 200 °C for more than 24 hours. Weight proportions of the starting materials are given in Table 1. The systems compositions were used based on the stoichiometry of the schematic reaction: $3Me^{2+}CO_3 + Al_2O_3 + 3SiO_2 \rightarrow Me_3^{2+}Al_2(SiO_4)_3 + 3CO_2$ (Me = Fe, Mg).

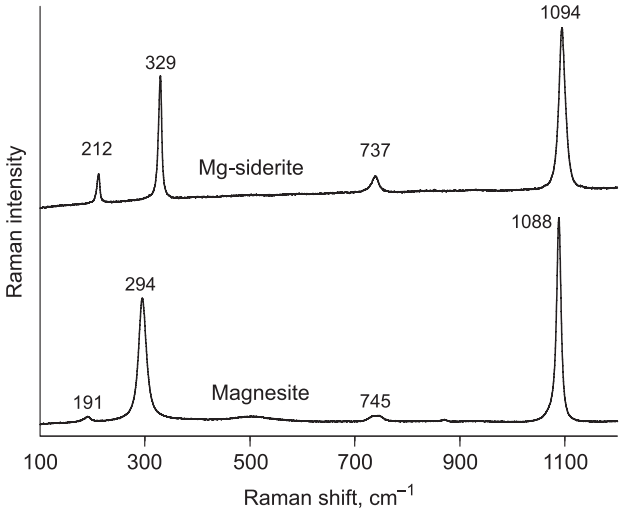

Fig. 3. Raman spectra of the starting natural magnesite and magnesiosiderite.

Methodological features of the assembly, the design of the high-pressure cell, as well as data on the features of the calibration were described elsewhere (Palyanov and Sokol, 2009; Sokol et al., 2015a,b). Considering the previous experience of experimental studies in carbonate-oxide systems (Pal'yanov et al., 2000, 2005), coupled with the generation of fluid in the initial solid-phase matrix, platinum was chosen as the material of the reaction ampoules. The volume of

Table 1. Weights of initial reagents

System	*P*, GPa	Weight, mg			
		Ms	MgSd	SiO_2	Al_2O_3
$MgCO_3$–SiO_2–Al_2O_3	3.0	4.8	–	3.3	1.9
	6.3	4.8	–	3.3	1.9
	7.5	3.8	–	2.7	1.5
(Mg,Fe)CO_3–SiO_2–Al_2O_3	3.0	0.9	4.3	3.1	1.8
	6.3	0.9	4.3	3.1	1.8
	7.5	0.7	3.4	2.4	1.4

Note: Ms, natural magnesite; MgSd, magnesiosiderite.

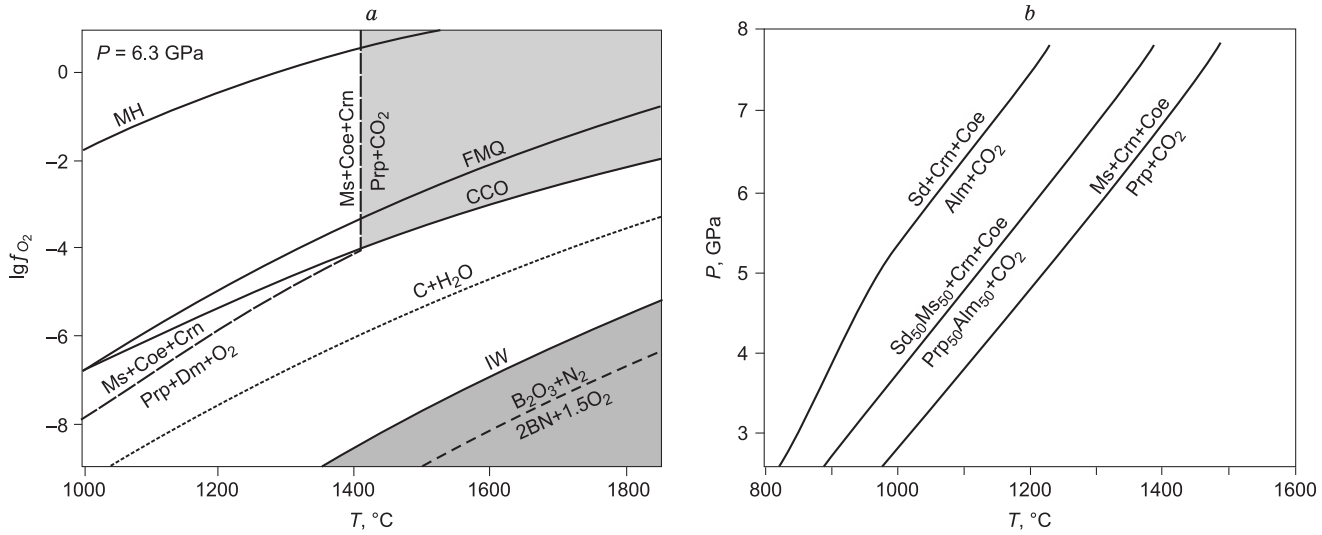

Fig. 4. T-f_{O_2} diagram (*a*) with lines of buffer equilibria, according to Robie et al. (1978); Holland and Powell (1990); Wendlandt et al. (1982), as well as the decarbonation reaction (Bataleva et al., 2012), and the *P–T* diagram (*b*) with the calculated theoretical positions of the decarbonation reactions to form pyrope, almandine and pyrope-almandine (Berman, 1991; Ogasawara et al., 1997). MH, magnetite-hematite; FMQ, fayalite-magnetite-quartz, IW, iron-wustite, CCO, buffer equilibria; Ms, magnesite, Coe, coesite, Crn, corundum, Prp, pyrope, Mgt, magnetite, Dm, diamond.

reaction ampoules is selected to ensure the implementation of the complex of necessary analytical studies, taking into account the size of the high-pressure cell. The internal size of the Pt ampoules for experiments at 3.0 and 6.3 GPa was 1.5 mm diameter with a length of 6 mm, and at 7.5 GPa it was 1.5 mm diameter with a length of 4 mm.

In the of high-temperature high-pressure experiments, the problem of hydrogen diffusion through the cell details and walls of reaction ampoules is well known (Boettcher et al., 1973; Luth, 1989). The result of this diffusion is a significant decrease in the oxygen fugacity in the reaction volume, leading to a shift of the decarbonation curves (Fig. 4*a*). In this study, to prevent the effect of hydrogen diffusion in the course of the experiments, we used a specially designed high-pressure cell with a hematite container (buffer) (Sokol et al., 2015b) (Fig. 5*a,b*). The effective working time of this container at temperatures below 1200 °C is at least 150 hours, and at 1500 °C it is about 5 hours. The duration of the experiments for each temperature is selected based on the time of effectiveness of the hematite container. After the experiments, control studies of the chemical composition of the hematite buffer container were carried out. In all cases, the material of the buffer container was represented by hematite and magnetite (± wustite), which indicates the effective work of the hematite container throughout the experiments. It should be noted that previous experiments on decarbonation with the formation of garnet (Knoche et al., 1999) were performed using boron nitride as a cell element, which sharply reduces oxygen fugacity in the samples (Fig. 4*a*) (Wendlandt et al., 1982; Luth, 1989), and does not allow adequately interpret the results.

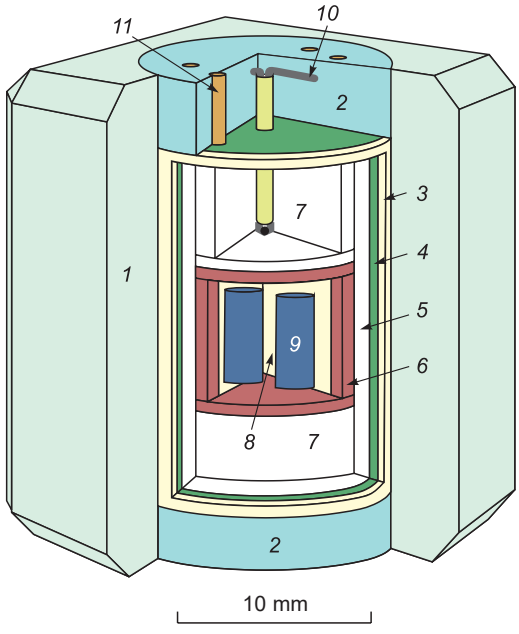

Fig. 5. Scheme of a high pressure cell: *1*, ZrO_2; *2*, talc ceramics; *3*, CsCl; *4*, graphite heater; *5*, MgO; *6*, hematite container; *7*, ZrO_2; *8*, CsCl; *9*, platinum ampoules; *10*, thermocouple $PtRh_6/PtRh_{30}$; *11*, Mo current leads.

The optimal P and T parameters of the experiments for both systems were selected based on published data of thermodynamic and thermochemical calculations, as well as experimental results (Berman, 1991; Ogasawara et al., 1997; Knoche et al., 1999; Pal'yanov et al., 2005). The theoretical position of decarbonation curves with the formation of almandine, pyrope-almandine and pyrope, calculated in this work, is shown in Fig. 4*b*.

Analytical research. The samples after the experiments were mounted in epoxy resin, sawn and polished. The phase and chemical compositions of the samples, as well as phase

relationships, were studied by optical methods (Carl Zeiss Axio Imager 2), electron scanning microscopy, and energy dispersive spectroscopy (TESCAN MIRA 3 LMU). Silicate phases were analyzed at an accelerating voltage of 20 kV, a probe current of 20 nA, a counting time of 10 seconds on each analytical line, and a probe diameter from an electron beam of 2–3 μm. The structural features of the obtained garnet crystals were studied by Raman spectroscopy (Jobin Yvon LabRAM HR800 spectrometer equipped with an Olympus BX41 stereo microscope). An He-Cd laser with a wavelength of 325 nm was used as an excitation source. To control the effectiveness of the hematite buffer, the composition of the fluid phase was qualitatively determined by mass spectrometry. For this, the platinum ampoule after the experiment was placed in a vacuum device connected to a sample injection system in a Delta V Advantage mass spectrometer and equipped with a special mechanism for piercing samples. After preliminary evacuation of the device with the sample to a pressure of 2.7·10–2 mbar, which guarantees the absence of atmospheric gases in the device, the ampoule was punctured and the gas released at room temperature was let into the mass spectrometer analyzer. Analytical studies were performed at the Analytical Center for multi-elemental and isotope research SB RAS.

EXPERIMENT RESULTS

The parameters and results of the experiments are presented in Table 2. The chemical compositions of the mineral phases are shown in Tables 3 and 4. Based on the previously developed approach and published results (Knoche et al., 1999), the most important criterion for the realization of the decarbonation reaction was considered to be garnet and CO_2 fluid formation accompanied either by a decrease in the amount of carbonate, or its complete consumption. It must be emphasized that the partial preservation of carbonate and oxides in the samples is a consequence of incomplete decarbonation reaction during the time of effective work of the hematite container (buffer).

$MgCO_3$–SiO_2–Al_2O_3 system. Experimental studies in the $MgCO_3$–SiO_2–Al_2O_3 system were carried out in the temperature ranges of 1050–1150 °C (3.0 GPa), 1100–1400 °C (6.3 GPa) and 1150–1450 °C (7.5 GPa). It has been demonstrated that in this system decarbonation occurs at 1100 ± 20 °C (3.0 GPa), 1150 ± 20 °C (6.3 GPa), and 1400 ± 20 °C (7.5 GPa). At the temperatures below the decarbonation reactions, the final samples are represented by recrystallized magnesite and oxides, as well as a small amount of newly formed kyanite (Fig. 6*a*). The formation of kyanite is established locally, at the contacts of corundum and coesite. At the temperatures above the decarbonation reaction (Fig. 6*b*-*e*), polycrystalline aggregates of pyrope, kyanite, and recrystallized starting materials are formed in the samples. Corundum, kyanite and pyrope form zonal aggregates of a rounded shape. In the central part of these aggregates, corundum is surrounded by kyanite crystals, and garnet forms rims in the peripheral part. Fluid cavities are commonly observed in the structure of samples. The composition of the obtained garnet in all experiments corresponds to the formula $Mg_{2.8\text{-}2.9}$

Table 2. Experimental parameters and results

Run N	System	*P*, GPa	*T*, °C	*t*, h.	Final mineral phases	Fluid composition*
1738-M	$MgCO_3$–$SiO_2Al_2O_3$	3.0	1050	60	Ms, Crn, Coe, Ky	–
2122-M	$MgCO_3$–$SiO_2Al_2O_3$	3.0	1150	60	Prp, Ky, Crn, Ms, Coe	CO_2
2117-M	$MgCO_3$–$SiO_2Al_2O_3$	6.3	1100	40	Ms, Crn, Coe, Ky	–
2119-M	$MgCO_3$–$SiO_2Al_2O_3$	6.3	1200	40	Ms, Crn, Coe, Ky	–
2115-M	$MgCO_3$–$SiO_2Al_2O_3$	6.3	1300	20	Prp, Coe, Ky, Crn, Ms	CO_2
2113-M	$MgCO_3$–$SiO_2Al_2O_3$	6.3	1400	10	Prp, Coe, Ky, Crn, Ms	n/a
2134-M	$MgCO_3$–$SiO_2Al_2O_3$	7.5	1150	60	Mgs, Coe, Ky	–
2139-M	$MgCO_3$–$SiO_2Al_2O_3$	7.5	1350	20	Ky, Coe, Crn, Ms	–
2140-M	$MgCO_3$–$SiO_2Al_2O_3$	7.5	1450	10	Prp, Coe, Ky, Crn, Ms	CO_2
1744-MF	(Mg,Fe)CO_3–SiO_2–Al_2O_3	3.0	950	60	Ky, Ms, Fms, MgSd, Coe	–
1738-MF	(Mg,Fe)CO_3–SiO_2–Al_2O_3	3.0	1050	60	Prp-Alm, Coe, Ky, Crn, Carb	CO_2
2117-MF	(Mg,Fe)CO_3–SiO_2–Al_2O_3	6.3	1100	40	Ky, Carb, Coe	–
2119-MF	(Mg,Fe)CO_3–SiO_2–Al_2O_3	6.3	1200	40	Prp-Alm, Ky, Carb, Crn	CO_2
2134-MF	(Mg,Fe)CO_3–SiO_2–Al_2O_3	7.5	1150	60	Carb, Crn, Coe, Ky	–
2136-MF	(Mg,Fe)CO_3–SiO_2–Al_2O_3	7.5	1250	40	Carb, Crn, Coe, Ky	–
2141-MF	(Mg,Fe)CO_3–SiO_2–Al_2O_3	7.5	1350	20	Carb, Crn, Coe, Ky	–
2144-MF	(Mg,Fe)CO_3–SiO_2–Al_2O_3	7.5	1450	10	Prp-Alm, Ky, Carb, Crn	CO_2

Note: Ms, magnesite; Fms, ferromagnesite; Carb, Mg,Fe-carbonates; MgSd, magnesiosiderite; Coe, coesite; Crn, corundum; Ky, kyanite; Prp, pyrope; Alm, almandine; n/a, not analyzed.
* analyzed by mass-spectrometry.

Table 3. Compositions of mineral phases in the $MgCO_3$-SiO_2-Al_2O_3 system

Run N	*P*, GPa	*T*, °C	Phase	Mass concentrations, wt.%							*n*(O)	Cations per formula unit						
				SiO_2	Al_2O_3	FeO	MgO	CaO	CO_2*	Total		Si	Al	Fe	Mg	Ca	C*	Σ cat
1738	3.0	1050	Ms	–	–	$0.5_{(1)}$	$44.0_{(3)}$	$0.8_{(6)}$	$54_{(2)}$	100.0	3	–	–	–	$0.95_{(1)}$	$0.02_{(1)}$	$1.02_{(1)}$	1.99
			Coe	$100.0_{(0)}$	–	–	0	–	–	100.0	2	$1.00_{(0)}$	–	–	–	–	–	1.00
2122		1150	Grt	$44.4_{(3)}$	$24.7_{(3)}$	$0.29_{(9)}$	$28_{(1)}$	$3_{(1)}$	–	99.6	12	$3.01_{(1)}$	$1.97_{(1)}$	–	$2.81_{(9)}$	$0.20_{(8)}$	–	8.00
			Ky	$34_{(1)}$	$66_{(2)}$	–	–	–	–	100.0	5	$0.88_{(8)}$	$2.2_{(1)}$	–	–	–	–	3.04
			Ms	–	–	$0.5_{(1)}$	$44.1_{(7)}$	$0.9_{(5)}$	$54_{(2)}$	100.0	3	–	–	–	$0.95_{(1)}$	$0.02_{(1)}$	$1.02_{(1)}$	1.99
			Crn	–	$100.0_{(0)}$	–	–	–	–	100.0	3	–	$2.00_{(0)}$	–	–	–	–	2.00
			Coe	$100.0_{(0)}$	–	–	–	–	–	100.0	2	$1.00_{(0)}$	–	–	–	–	–	1.00
2117	6.3	1100	Ky	$36.0_{(3)}$	$63.8_{(5)}$	–	–	$0.2_{(1)}$	–	100.2	5	$1.00_{(0)}$	$2.00_{(0)}$	–	–	–	–	3.01
			Ms	–	–	$0.5_{(0)}$	$42_{(1)}$	$1.2_{(8)}$	$55.1_{(1)}$	100.0	3	–	–	$0.01_{(0)}$	$0.88_{(2)}$	$0.02_{(1)}$	$1.01_{(0)}$	1.96
			Coe	100	–	–	–	–	–	100.0	2	1.00	–	–	–	–	–	3.00
2119		1200	Ky	$35_{(2)}$	$61_{(4)}$	–	–	–	–	99.3	5	$0.98_{(6)}$	$2.0_{(1)}$	–	–	–	–	3.03
			Ms	–	–	$0.7_{(3)}$	$43.5_{(3)}$	$0.5_{(1)}$	$55.3_{(1)}$	100.0	3	–	–	$0.01_{(0)}$	$0.90_{(1)}$	$0.01_{(0)}$	$1.04_{(1)}$	1.96
			Coe	$100_{(0)}$	–	–	–	–	–	100.0	2	$1.00_{(0)}$	–	–	–	–	–	3.00
2115		1300	Grt	$44.4_{(2)}$	$24.2_{(2)}$	$1.6_{(3)}$	$27.5_{(1)}$	$1.7_{(3)}$		99.5	12	$3.03_{(1)}$	$1.95_{(2)}$	$0.09_{(2)}$	$2.80_{(1)}$	$0.12_{(2)}$	–	8.00
			Ky	$35.9_{(8)}$	$63.6_{(6)}$	–	–	–	–	99.5	5	$0.98_{(2)}$	$2.04_{(2)}$	–	–	–	–	3.01
			Crn	–	$100.0_{(0)}$	–	–	–	–	100.0	3	–	2.00	–	–	–	–	2.01
			Coe	$100.0_{(0)}$	–	–	–	–	–	100.0	2	$1.00_{(0)}$	–	–	–	–	–	1.00
			Ms	–	–	$0.6_{(4)}$	$43.4_{(3)}$	$1.2_{(5)}$	$54.8_{(2)}$	100.0	3	–	–	$0.01_{(0)}$	$0.90_{(1)}$	$0.02_{(1)}$	$1.01_{(0)}$	1.96
2113		1400	Grt	$45.0_{(4)}$	$24.4_{(4)}$	$0.4_{(1)}$	$24.5_{(2)}$	$1.9_{(2)}$	–	100.2	12	$3.03_{(1)}$	$1.94_{(2)}$	$0.02_{(1)}$	$2.86_{(2)}$	$0.14_{(2)}$	–	8.02
			Ky	$35_{(2)}$	$64_{(1)}$	–	–	–	–	99.4	5	$0.96_{(3)}$	$2.05_{(3)}$	–	–	–	–	3.02
			Crn	–	$99_{(1)}$	–	–	–	–	99.4	3	–	$1.99_{(1)}$	–	–	–	–	1.98
			Ms	–	–	$0.5_{(1)}$	$43.2_{(4)}$	$1.4_{(4)}$	$55.0_{(4)}$	100.0	3	–	–	–	$0.97_{(1)}$	$0.02_{(1)}$	$1.03_{(2)}$	1.97
			Coe	$100.0_{(0)}$	–	–	–	–	–	100.0	2	$1.00_{(0)}$	–	–	–	–	–	1.00
2134	7.5	1150	Ms	–	–	$0.62_{(5)}$	$47_{(2)}$	$2.1_{(6)}$	$51_{(2)}$	100.0	3	–	–	$0.01_{(0)}$	$0.98_{(6)}$	$0.03_{(1)}$	$0.98_{(2)}$	2.01
			Ky	$37.9_{(0)}$	$61.8_{(0)}$	–	–	$0.3_{(0)}$	–	100.0	5	$1.02_{(0)}$	$1.97_{(0)}$	–	–	$0.01_{(0)}$	–	3.00
			Coe	$100.0_{(0)}$	–	–	–	–	–	100.0	2	$1.00_{(0)}$	–	–	–	–	–	1.00
2139		1350	Ky	$35_{(2)}$	$65_{(2)}$	–	–	–	–	99.4	5	$0.94_{(6)}$	$2.08_{(8)}$	–	–	–	–	3.02
			Ms	–	–	$0.8_{(3)}$	$43_{(2)}$	$1.2_{(7)}$	$54_{(2)}$	100.0	3	–	–	$0.01_{(0)}$	$0.91_{(4)}$	$0.02_{(1)}$	$1.03_{(2)}$	1.96
			Crn	–	$100.0_{(0)}$	–	–	–	–	100.0	3	–	$2.00_{(0)}$	–	–	–	–	2.00
			Coe	$100.0_{(0)}$	–	–	–	–	–	100.0	2	$1.00_{(0)}$	–	–	–	–	–	1.00
2140		1450	Grt	$45.0_{(1)}$	$24.5_{(3)}$	$0.6_{(1)}$	$28.1_{(3)}$	$1.5_{(1)}$	–	99.6	12	$3.05_{(0)}$	$1.94_{(1)}$	$0.03_{(0)}$	$2.86_{(2)}$	$0.11_{(1)}$	–	7.97
			Ky	$37_{(3)}$	$62_{(3)}$	–	–	–	–	99.5	5	$1.01_{(7)}$	$2.0_{(1)}$	–	–	–	–	3.01
			Crn	–	$100.0_{(0)}$	–	–	–	–	100.0	3	–	$2.00_{(0)}$	–	–	–	–	2.00
			Coe	$100.0_{(0)}$	–	–	–	–	–	100.0	2	$1_{(0)}$	–	–	–	–	–	1.00
			Ms	–	–	$0.4_{(1)}$	$43.3_{(7)}$	$1.2_{(1)}$	$55.0_{(6)}$	100.0	3	–	–	$0.01_{(0)}$	$0.89_{(0)}$	$0.02_{(0)}$	$1.04_{(1)}$	1.96

Note: Ms, magnesite; Coe, coesite; Crn, corundum; Ky, kyanite; Grt, pyrope.
* calculated after sum deficit.

$Ca_{0.05\text{-}0.12}Fe_{0.05\text{-}0.09}Al_{1.95}Si_{3.03}O_{12}$. With increasing pressure in the synthesized garnets, the number of formula units of silicon increases from 3.03 at 6.3 GPa to 3.05 at 7.5 GPa (when converted to 12 formula units of oxygen). Together with this, an increase in the deficit of aluminum cations in the octahedral position is observed: from 1.95 (6.3 GPa) to 1.94 (7.5 GPa). Based on these facts, we can say that the garnet obtained contains a majoritic component, the proportion of which increases with increasing pressure from 2.5 to 3 mol.%. In the Raman spectra of the resulting pyrope, the main modes are 364, 562, 924–925 cm^{-1} (Fig. 7*a*; Table 5).

$(Mg,Fe)CO_3$–SiO_2–Al_2O_3 system. Experimental studies in the $(Mg,Fe)CO_3$–SiO_2–Al_2O_3 system were carried out in the temperature ranges of 950–1050 °C (3.0 GPa), 1100–1200 °C (6.3 GPa) and 1150–1450 °C (7.5 GPa). It has been experimentally demonstrated that decarbonation occurs in this system at 1000 ± 20 °C (3.0 GPa), 1150 ± 20 °C (6.3 GPa), and 1400 ± 20 °C (7.5 GPa). At the temperatures below the implementation of the decarbonation reactions, the obtained samples are represented by the assemblage of Mg,Fe-carbonates of various compositions (magnesite, ferromagnesite, magnesiosiderite (Table 4)), recrystallized starting oxides

Table 4. Compositions of mineral phases in the (Mg,Fe)CO_3–SiO_2–Al_2O_3 system

Run N	P, GPa	T, °C	Phase	Mass concentrations. wt.%								n(O)	Cations per formula unit							
				SiO_2	Al_2O_3	FeO	MnO	MgO	CaO	CO_2*	Total		Si	Al	Fe	Mn	Mg	Ca	C*	Σcat
1744–MF	3.0	950	Ky	$36.2_{(9)}$	$62.5_{(1)}$	$1.4_{(7)}$	–	–	–	–	100.0	5	$0.99_{(1)}$	$2.00_{(4)}$	$0.03_{(1)}$	–	–	–	–	3.02
			Ms	–	–	$1.02_{(4)}$	–	$44.8_{(4)}$	$0.6_{(2)}$	$53.6_{(4)}$	100.0	3	–	–	$0.01_{(0)}$	–	$0.94_{(1)}$	$0.01_{(0)}$	$1.03_{(1)}$	1.98
			Fms	–	–	$19_{(6)}$	$0.5_{(1)}$	$32_{(5)}$	$2.5_{(5)}$	$47_{(2)}$	100.0	3	–	–	$0.2_{(1)}$	$0.01_{(0)}$	$0.72_{(7)}$	$0.04_{(1)}$	$0.97_{(3)}$	2.01
			MgSd	$0.2_{(0)}$	$0.3_{(0)}$	$41_{(2)}$	$0.8_{(1)}$	$15_{(2)}$	$0.4_{(1)}$	$42.2_{(9)}$	100.0	3	–	–	$0.60_{(4)}$	$0.01_{(0)}$	$0.39_{(5)}$	$0.01_{(0)}$	$0.99_{(2)}$	2.01
			Coe	$99.8_{(5)}$	–	$0.8_{(3)}$	–	–	–	–	100.6	2	$1.00_{(0)}$	–	–	–	–	–	–	1.00
1739–MF	3.0	1050	Grt	$39_{(2)}$	$22_{(3)}$	$28.3_{(2)}$	–	$8.2_{(6)}$	$2.0_{(0)}$	–	100.3	12	$3.0_{(2)}$	$2.0_{(2)}$	$1.83_{(1)}$	–	$0.94_{(5)}$	$0.17_{(0)}$	–	8.01
			Carb	–	–	$32_{(2)}$	$0.6_{(1)}$	$24_{(1)}$	$1.0_{(2)}$	$43_{(1)}$	100.0	3	–	–	$0.43_{(3)}$	$0.01_{(0)}$	$0.58_{(2)}$	$0.02_{(1)}$	$0.97_{(1)}$	2.02
			Crn	–	$98.6_{(2)}$	$2.0_{(2)}$	–	–	–	–	100.6	3	–	$1.98_{(0)}$	$0.03_{(0)}$	–	–	–	–	2.00
			Coe	99.6	–	0.8	–	–	–	–	100.4	2	$1_{(0)}$	–	$0.01_{(0)}$	–	–	–	–	1.00
2117–MF	6.3	1100	Ky	$34.5_{(3)}$	$65_{(1)}$	$1.0_{(1)}$	–	–	–	–	100.3	5	$0.94_{(2)}$	$2.07_{(2)}$	$0.02_{(0)}$	–	–	–	–	3.03
			Carb	–	–	$41_{(2)}$	$0.7_{(0)}$	$15_{(1)}$	$0.4_{(1)}$	$41.8_{(3)}$	100.0	3	–	–	$0.60_{(4)}$	$0.01_{(0)}$	$0.40_{(3)}$	$0.01_{(0)}$	$0.99_{(1)}$	2.01
			Coe	$99.4_{(1)}$	–	$0.6_{(1)}$	–	–	–	–	100.0	2	$1.00_{(0)}$	–	–	–	–	–	–	1.01
2119–MF	6.3	1200	Grt	$38.7_{(3)}$	$21.5_{(3)}$	$28.3_{(6)}$	$0.7_{(1)}$	$8.8_{(2)}$	$1.8_{(2)}$	–	99.8	12	$3.00_{(2)}$	$1.97_{(2)}$	$1.84_{(4)}$	$0.05_{(1)}$	$1.01_{(3)}$	$0.15_{(2)}$	–	8.02
			Ky	$35.9_{(8)}$	$62_{(2)}$	$1.7_{(8)}$	–	–	–	–	99.5	5	$0.99_{(2)}$	$1.99_{(5)}$	$0.04_{(2)}$	–	$0.01_{(1)}$	–	–	3.02
			Carb	–	–	$28.7_{(8)}$	$0.51_{(4)}$	$24_{(1)}$	$1.2_{(0)}$	$44.6_{(9)}$	100.0	3	–	–	$0.39_{(1)}$	$0.01_{(0)}$	$0.59_{(2)}$	$0.02_{(0)}$	$0.99_{(1)}$	2.01
			Crn	–	$98_{(1)}$	$1.2_{(1)}$	–	–	–	–	100.3	3	–	$1.95_{(4)}$	$0.02_{(0)}$	–	–	–	–	2.00
2136–MF	7.5	1250	Ky	$36.4_{(1)}$	$61.9_{(1)}$	$1.2_{(1)}$	–	–	–	–	99.5	5	$0.99_{(0)}$	$1.99_{(0)}$	$0.03_{(0)}$	–	–	–	–	3.01
			Carb	–	–	$38_{(6)}$	$0.8_{(1)}$	$18_{(3)}$	–	$43_{(2)}$	100.0	3	–	–	$0.49_{(9)}$	$0.01_{(0)}$	$0.45_{(7)}$	–	$0.97_{(4)}$	2.01
			Coe	$100.0_{(1)}$	–	$0.7_{(0)}$	–	–	–	–	100.7	2	$1.00_{(0)}$	–	$0.01_{(0)}$	–	–	–	–	1.00
2141–MF	7.5	1350	Ky	$36.4_{(6)}$	$61.0_{(5)}$	$3.2_{(6)}$	–	–	–	–	100.6	5	$1.00_{(2)}$	$1.96_{(1)}$	$0.07_{(1)}$	–	–	–	–	3.03
			Carb	–	–	$34_{(5)}$	$0.6_{(1)}$	$20_{(3)}$	$1.0_{(4)}$	$44_{(1)}$	100.0	3	–	–	$0.48_{(8)}$	$0.01_{(0)}$	$0.50_{(7)}$	$0.02_{(0)}$	$1_{(0)}$	2.00
			Crn	–	$95.1_{(6)}$	$3.4_{(3)}$	–	–	–	–	99.4	3	–	$1.95_{(2)}$	$0.05_{(0)}$	–	–	–	–	2.01
			Coe	$99.6_{(1)}$	–	$0.6_{(1)}$	–	–	–	–	100.2	2	$1.00_{(0)}$	–	$0.01_{(0)}$	–	–	–	–	1.01
2144–MF	7.5	1450	Grt	$38.9_{(7)}$	$21.2_{(4)}$	$28.7_{(9)}$	$0.7_{(1)}$	$8.9_{(4)}$	$1.4_{(1)}$	–	100.1	12	$3.02_{(2)}$	$1.94_{(2)}$	$1.86_{(8)}$	$0.05_{(1)}$	$1.03_{(4)}$	$0.11_{(1)}$	–	8.01
			Ky	$36.5_{(1)}$	$60.7_{(1)}$	$3.5_{(1)}$	–	–	–	–	100.7	5	$0.99_{(0)}$	$1.95_{(0)}$	$0.08_{(0)}$	–	–	–	–	3.02
			Carb	–	–	$28_{(2)}$	$0.5_{(1)}$	$23.9_{(5)}$	$1.1_{(1)}$	$46_{(2)}$	100.0	3	–	–	$0.38_{(4)}$	$0.01_{(0)}$	$0.57_{(1)}$	$0.02_{(0)}$	$1.02_{(3)}$	1.99

Note: Ms, magnesite; Carb, Mg,Fe-carbonate; Coe, coesite; Crn, corundum; Ky, kyanite; Grt, pyrope-almandine;
* calculated after sum deficit.

and newly formed kyanite (Fig. 8*a-c*). At the temperatures of the onset of decarbonation reactions and higher, the formation of pyrope-almandine garnet and kyanite, as well as recrystallized starting oxides and Mg,Fe-carbonates, was established in the samples (Fig. 8*d-f*). As in the $MgCO_3$–SiO_2–Al_2O_3 system, corundum, kyanite, and pyrope form zonal aggregates. A large number of fluid cavities were found in the samples. The composition of the pyrope-almandine corresponds to the formulas $(Fe_{1.83}Mg_{0.94}Ca_{0.17})Al_2(SiO_4)_3$ (3.0 GPa), $(Fe_{1.84}Mg_{1.01}Ca_{0.15}Mn_{0.05})Al_{1.97}(SiO_4)_3$ (6.3 GPa) and $(Fe_{1.86}Mg_{1.03}Ca_{0.11}Mn_{0.05})Al_{1.94}(Si_{3.02}O_{12})$ (7.5 GPa). An increase in the number of formula units of silicon is noted – from 3.0 (6.3 GPa) to 3.03 (7.5 GPa), accompanied by an increase in the deficiency of Al cations in the octahedral position: from 1.97 (6.3 GPa) to 1.94 (7.5 GPa) were established with pressure. Based on these data, it was found that the proportion of majoritic component in the synthesized garnets increases with increasing pressure from 0 to ~ 3 mol.%. However, it should be noted that the deficiency of aluminum in the garnets of this system can be also caused by the entry of ferric iron. The Raman spectra of pyrope-almandine are characterized by the most intense modes 350–351, 556–558, and 918–919 cm^{-1} (Fig. 7*b*, Table 5).

The formation of CO_2 fluid. As shown above, in $MgCO_3$–SiO_2–Al_2O_3 and (Mg,Fe)CO_3–SiO_2–Al_2O_3 systems at temperatures exceeding the temperature of the onset of decarbonation, the fluid cavities (Figs. 6*f*, 8*e,f*) formed as a result of segregation CO_2 fluid. The cavity sizes are from 10 to 300 microns. It should be noted that coesite crystals with their own faceting were found on the walls of some fluid cavities (Fig. 6*f*). In previous studies, during which decarbonation reactions were experimentally reproduced (Palyanov et al., 2007; Bataleva et al., 2016), it was demonstrated that CO_2 fluid at mantle pressures and temperatures is capable of dissolving and transporting oxides, carbonates and silicates. In the present study, in a number of experiments, the composition of the fluid in the obtained samples was controlled by mass spectrometry. During the study, scanning the mass range from 12 to 46 a.e.m. revealed the presence of peaks at masses 44, 45, and 46, which correspond exclusively to CO_2 (signals at other masses did not

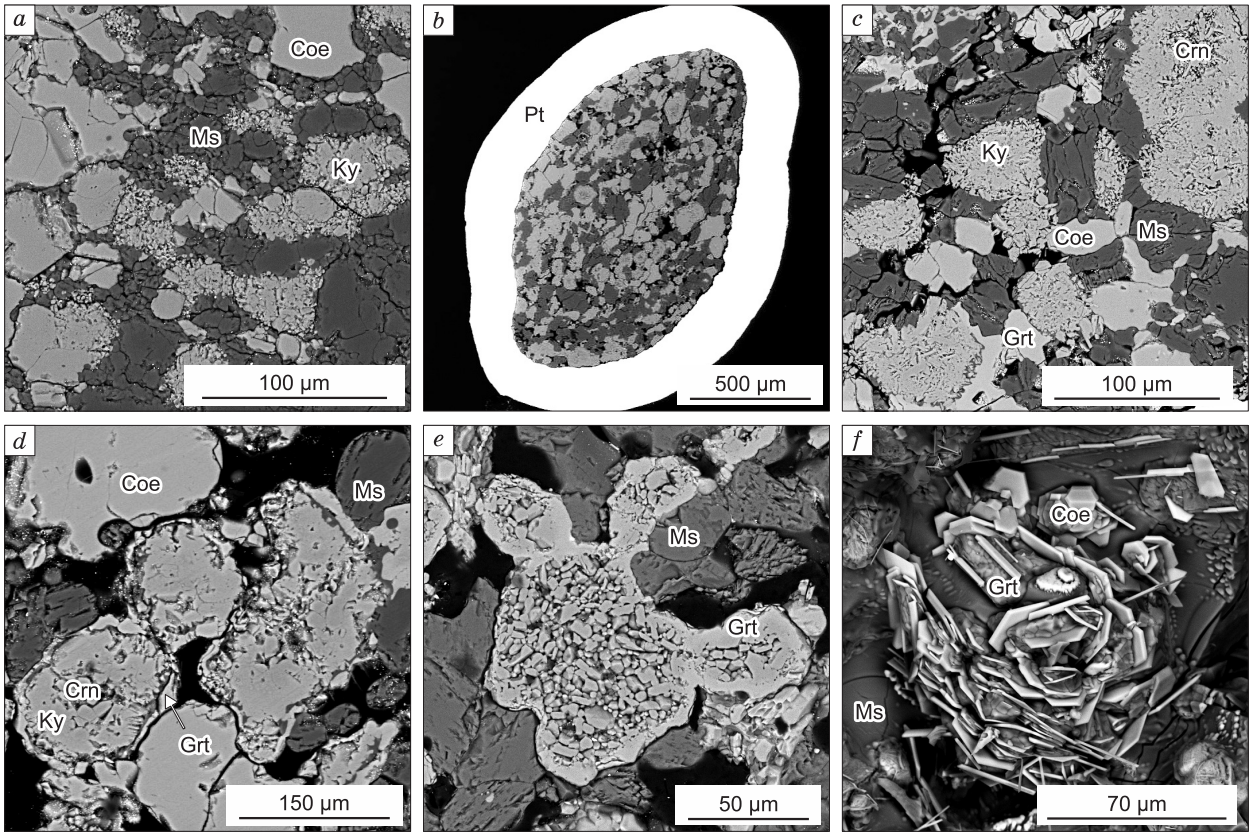

Fig. 6. SEM micrographs of polished fragments (*a*-*e*) and cleaves (*e*) of samples obtained in the $MgCO_3$–SiO_2–Al_2O_3 system: *a*, Polycrystalline aggregate of newly formed kyanite and recrystallized coesite and magnesite (6.3 GPa, 1100 °C); *b*, a platinum ampoule with a sample after the experiment at 1150 °C and 3.0 GPa; *c*, polycrystalline aggregate of newly formed garnet and kyanite and recrystallized starting oxides and magnesite (1150 °C, 3.0 GPa); *g*–*d*, garnet crystals and rims (1400 °C, 6.3 GPa); *e*, crystals of coesite and garnet on the wall of the fluid cavity (1400 °C, 6.3 GPa); Ms, magnesite; Coe, coesite; Crn, corundum; Ky, kyanite; Grt, pyrope.

exceed background values). Thus, it was found that in all samples, both in relatively low and high temperature, the fluid composition corresponded to pure CO_2, without impurities of hydrogen or H_2O. These data indicate the effectiveness of the hematite buffer and adequate experimental results.

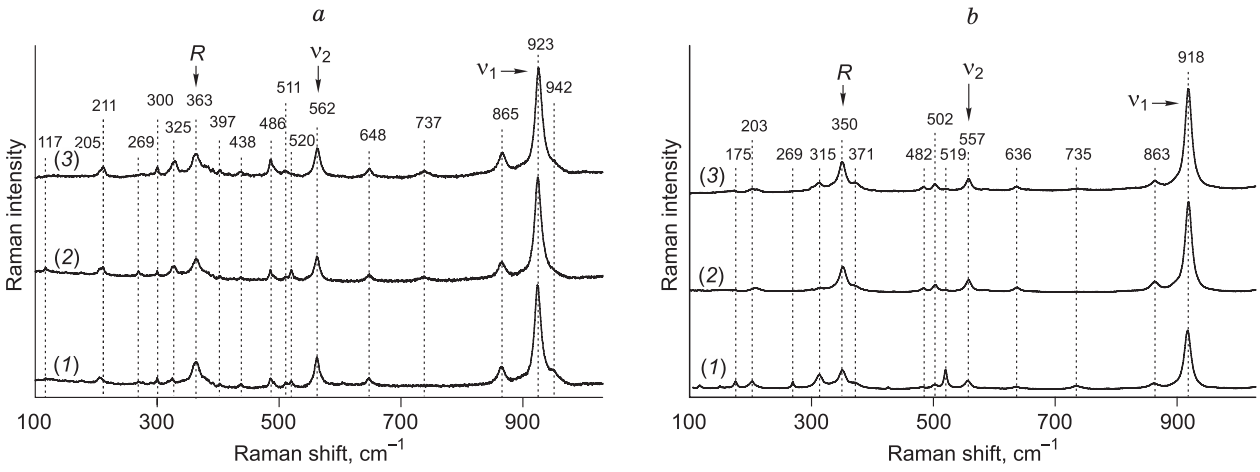

Fig. 7. Representative Raman spectra of the obtained pyrope (*a*), *1,2*, No. 2113-M, *3*, No. 2140-M and pyrope-almandine (*b*), *1,2*, No. 1738-MF, *3*, No. 2119-MF.

Table 5. Raman spectroscopic characteristics of synthesized Mg,Fe–garnets

Run No	*P*, GPa	*T*, °C	Phase	Raman spectroscopic characteristics (wavenumber, cm^{-1})																					
				$R(SiO_4)^{4-}$												$(Si–O)_{def}$, υ_2						$(Si–O)_{val}$, υ_1			
2140–M	7.5	1450	Prp	–	116	–	176	211	273	300	–	328	–	364	403	437	486	–	510	520	562	–	647	–	866	–	925	–	1061
2113–M	6.3	1400	Prp	–	116	–	173	205	277	300	–	325	–	364	403	438	486	–	511	520	562	–	648	–	864	–	924	–	1061
2113–M	6.3	1400	Prp	–	118	144	178	211	269	300	–	325	–	364	398	438	486	–	–	520	562	–	648	–	865	–	925	–	1061
2119–MF	6.3	1200	Prp–Alm	–	–	–	174	205	–	–	312	–	350	371	–	–	485	502	–	–	558	637	–	736	863	918	–	1047	–	
1738–MF	3.0	1050	Prp–Alm	–	117	150	176	203	269	–	313	–	350	–	–	426	482	–	–	520	556	636	–	736	864	918	–	1045	–	
1738–MF	3.0	1050	Prp–Alm	105	–	–	–	209	–	–	315	–	351	–	–	–	490	503	–	–	557	638	–	–	863	919	–	1047	–	
Prp*	–	–	Prp	–	135	–	–	211	284	–	–	–	344	364	375	–	–	–	–	525	563	626	–	–	871	–	928	–	1066	
Alm*	–	–	Alm	–	–	–	171	216	256	–	314	323	342	370	–	–	475	500	–	521	581	630	–	–	863	916	–	1038	–	

Note: * Kolesov, Geiger, 1998; Prp, pyrope; Alm, almandine.

DISCUSSION

Features of the obtained Mg,Fe garnets. Currently, there are a large number of studies of garnet-bearing mantle rocks. Garnets from xenoliths of kimberlites, Mg-enriched peridotites, Fe-enriched peridotites and pyroxenites, eclogites, megacrysts, and inclusions in P- and E-type diamonds have been studied in most detail (Sobolev et al., 1969, 1973, 1998, 2016, 2019; Sobolev, 1970, 1977; Gurney and Switzer, 1973; Gurney et al., 1979, 1991; Gurney and Harte, 1980; Harris, 1987, 1992; Meyer, 1987; Harte and Hawkesworth, 1989; Boyd et al., 1993; Griffin et al., 1999; Kopylova et al., 1999; Pearson et al., 2003; Kalugina and Zedgenizov, 2019). Moreover, harzburgite and eclogite garnets are often associated with diamond (Sobolev et al., 1973, 1998; Pokhilenko et al., 1993). The garnets obtained by us in terms of Me^{2+} contents are the closest to pyropes and pyrope-almandines of Fe-enriched peridotites and pyroxenites, as well as carbonated eclogites.

Using the Raman spectroscopy method, the obtained crystals of pyrope and pyrope-almandine were characterized, as well as a comparative study of these garnets was performed (Fig. 7; Table 5). A comparison of the obtained spectra with each other, as well as a comparison with the available literature data, made it possible to reveal the key spectroscopic characteristics of garnets obtained as a result of decarbonation reactions at mantle pressures and temperatures. The main characteristic of the Raman spectra of natural pyrope and almandine are the modes near 350, 550, and 900 cm^{-1}, which are related to librational ($R(SiO4)^{4-}$), intrinsic deformation ($(Si-O)_{def}$, υ_2), and valence ($(Si-O)_{val}$, υ_1) vibrations of the SiO_4 tetrahedron, respectively (Kolesov and Geiger, 1998). In particular, the Raman spectra of chemically pure pyrope show the most intense peaks of 364, 563, 928 cm^{-1}, and peaks of 342, 556, and 916 cm^{-1} are characteristic of almandine (Kolesov and Geiger, 1998). In the present study, it was experimentally established that the most intense peaks in the spectra of pyrope formed as a result of decarbonation reactions are 364, 562, 924–925 cm^{-1}, and in the spectra of pyrope-almandine – 350–351, 556–558 and 918–919 cm^{-1} (Table 5).

In the studies (Kolesov and Geiger, 1998; Kalugina and Zedgenizov, 2019) it was demonstrated that garnet solid solutions are characterized by successive unilateral shifts of the main modes with an increase in the concentration of one of the minals. The shifts of the *R*, υ_2, and υ_1 modes to the higher-frequency region relative to the pyrope by 13–14 cm^{-1}, 4–6 cm^{-1}, and 6 cm^{-1}, respectively, were established in the pyrope-almandine obtained by us. Secondary peaks 116-118, 144, 173-178, 269-277, 300, 325-328, 398 should be noted as secondary modes characteristic of pyrope formed as a result of decarbonation reactions and not established in the Raman spectra of chemically pure pyrope 403 and 647 cm^{-1}. For pyrope-almandine, these are peaks 117, 150, 350, 426, and 736 cm^{-1}. When comparing the Raman

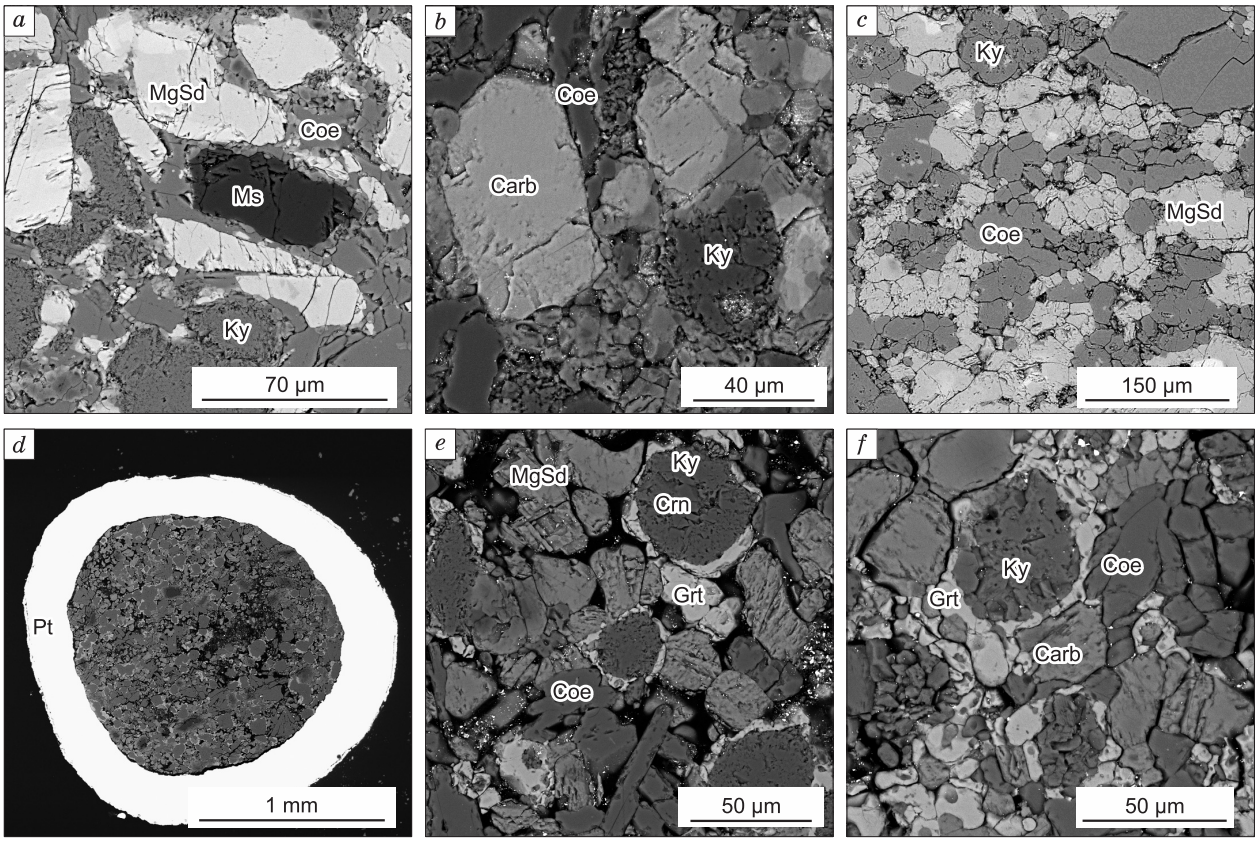

Fig. 8. SEM micrographs of polished fragments of samples obtained in the system (Mg,Fe)CO_3–SiO_2–Al_2O_3: *a–c,* Polycrystalline aggregate of newly formed kyanite and recrystallized coesite and carbonates (*a*, 3.0 GPa, 950 °C; *b*, 6.3 GPa, 1100 °C; *c*, 7.5 GPa, 1250 °C); *g*, platinum ampoule with the sample after the experiment at 1050 °C and 3.0 GPa; *d*, a polycrystalline aggregate of newly formed garnet and kyanite and recrystallized starting oxides and magnesiosiderite (1050 °C and 3.0 GPa); *f*, garnet crystals and rims (1400 °C, 7.5 GPa); Ms, magnesite; Carb, Mg, Fe-carbonate of variable composition; MgSd, magnesiosiderite; Coe, coesite; Crn, corundum; Ky, kyanite; Grt, pyrope-almandine garnet.

characteristics of the obtained pyrope and almandine pyrope with inclusions of different paragenesis in diamonds (Kalugina and Zedgenizov, 2019), the greatest similarity was found with E-type garnets, with the main modes in the intervals of 355.9–361.2 cm^{-1} for *R*, 554.5–558.7 cm^{-1} for υ_2 and 907.5–918.1 cm^{-1} for υ_1.

Reconstruction of decarbonation reactions with the formation of the association of Mg,Fe-garnets + CO_2 in the *P–T* field. According to modern concepts, under conditions of subduction of crustal material to great depths, oxidized slab is a source of carbonates, carbonate melts and the CO_2 fluid (Plank and Manning, 2019). Information on the conditions for the formation of the CO_2 fluid is very important, since its presence, even in small amounts, can lead to sharp changes in melting parameters and initiation of mantle metasomatic processes (Kadik and Lukanin, 1986; Pal'yanov et al., 2000; Foley, 2010; Perchuk et al., 2019). It is under subduction conditions that the most characteristic are decarbonation reactions that occur during the interaction of a carbonate material with mantle oxides or silicates. However, subducted Mg–Ca carbonates can be stable to the depths of the lower mantle (Brenker et al., 2007; Boulard et al., 2011; Merlini et al., 2012; Oganov et al., 2013). As shown in (Berman, 1991; Martin and Hammouda, 2011; Bataleva et al., 2016), the presence of iron can significantly reduce the temperature of the onset of decarbonation reactions and trigger the formation of CO_2 fluid and ferruginous silicates. In this study, it was demonstrated that magnesiosiderite at pressures of 3.0 and 6.3 GPa enters the decarbonation reaction at temperatures 100 °C lower than magnesite, and at a pressure of 7.5 GPa decarbonation parameters involving Mg and Mg, Fe carbonates almost identical. Thus, when considering the results obtained with regard to the stability of natural carbonates of various compositions under subduction conditions, it was found that at depths of ~ 90–190 km Mg,Fe-carbonates react with oxides in the temperature range 1000–1250 °C, and at depths ~ 225 km – at 1400 °C.

As a result of a detailed study of the obtained experimental data, the position of the decarbonation curves was reconstructed, leading to the formation of a CO_2 fluid in association with pyrope (Fig. 9*a*) and pyrope-almandine (Fig. 9*b*) in a *P–T* field. A comparison of the positions of the calculated decarbonation curves and the experimental results showed that the experimentally reproduced reaction lines are predominantly shifted to lower temperatures relative to the calculated ones, and in some cases practically coincide

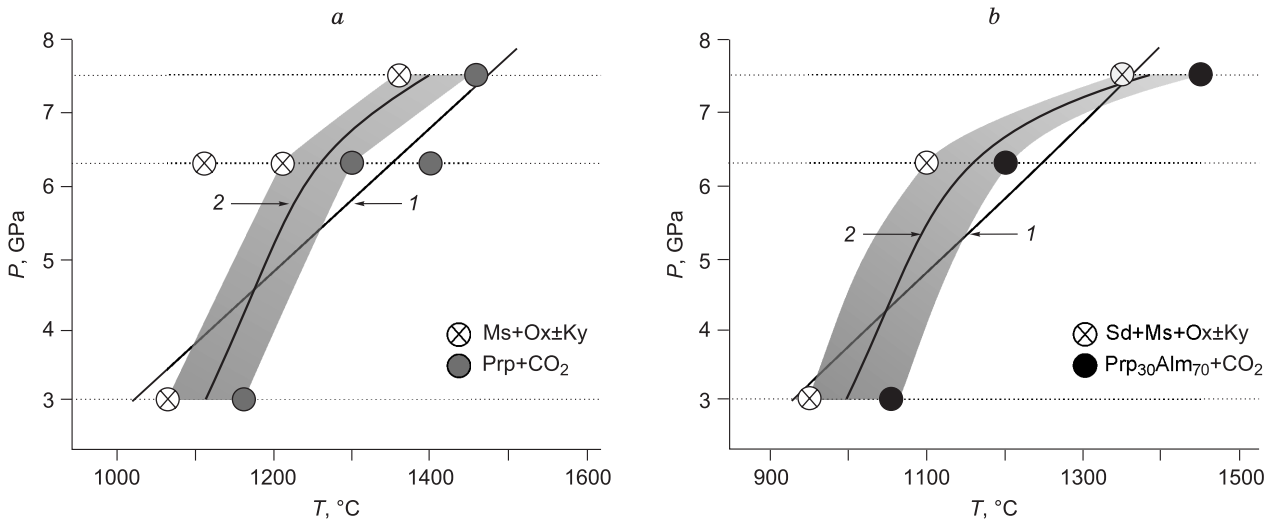

Fig. 9. *P–T* diagrams with theoretically calculated (*1*) and experimentally determined (*2*) in this work, decarbonization reactions associated with the formation of CO_2 fluid and (*a*) pyrope and (*b*) pyrope-almandine. Ms, magnesite; Ox, oxides (corundum ± coesite); Ky, kyanite; Prp, pyrope; Alm, almandine.

with them. The difference between the calculated and experimentally determined decarbonation temperatures for the $MgCO_3$–SiO_2–Al_2O_3 system can be 50–150 °C, and for the (Mg,Fe)CO_3–SiO_2–Al_2O_3 system, it can be from 0 to 100 °C.

The experimentally determined specific stability temperatures of carbonate-oxide associations and the boundary crystallization conditions of Mg,Fe-garnets in a *P–T* field make it possible to understand the conditions for the generation of fluid in the initial solid-phase matrix, as well as to evaluate the *P–T* stability regions of natural Mg,Fe-carbonates in association with oxides. When comparing the available data on the melting points of natural magnesite and magnesiosiderite ($Sd_{50}Mg_{50}$) (Fig. 1) (Tao et al., 2013; Shatskiy et al., 2015; Kang et al., 2016; Shatskiy et al., 2018) with the decarbonation temperatures of Mg,Fe-carbonate-oxide associations, the following laws were established. Magnesite enters the decarbonation reaction at temperatures 400 °C (3.0 GPa), 650 °C (6.3 GPa) and 500 °C (7.5 GPa) below its melting points. Decarbonation reactions involving magnesiosiderite occur at temperatures 300 °C (3.0 GPa), 450 °C (6.3 GPa) and 200 °C (7.5 GPa) below its melting points. Thus, the data obtained demonstrate that decarbonation reactions can lead to the formation of CO_2 fluid, one of the most powerful metasomatic agents, at temperatures hundreds of degrees lower than the temperatures of formation of carbonate melts, which is critical information in the framework of the complex problem of reconstruction of fluid processes, global carbon cycle, and mantle metasomatism under subduction conditions.

CONCLUSIONS

1. Experimental modeling of decarbonation reactions coupled with the formation of Mg,Fe-garnets and a CO_2 fluid was carried out at the *P–T* parameters of the upper mantle. In an experimental study using a specially designed high-pressure cell with a hematite container that prevents hydrogen diffusion into the sample, it was found that in the $MgCO_3$–SiO_2–Al_2O_3 system decarbonation occurs at 1100 ± 20 °C (3.0 GPa), 1150 ± 20 °C (6.3 GPa), and 1400 ± 20 °C (7.5 GPa), and in the system (Mg,Fe)CO_3–Al_2O_3–SiO_2 – at 1000 ± 20 °C (3.0 GPa), 1150 ± 20 °C (6.3 GPa), and 1400 ± 20 °C (7.5 GPa).

2. Using the method of mass spectrometry, the effective work of the hematite container was demonstrated, and it was found that in all experiments the composition of the fluid corresponded to pure CO_2.

3. The Raman spectroscopic characterization of the garnets obtained was performed and the position of the main modes *R*, υ_2 and υ_1 in the pyrope was determined – 364, 562, 924–925 cm^{-1}, and pyrope-almandine – 350–351, 556–558 and 918–919 cm^{-1}.

4. An experimental reconstruction of the position of the decarbonation curves, leading to the formation of a CO_2 fluid and pyrope or pyrope-almandine, was carried out. It was found that experimentally determined reaction lines with the formation of the pyrope + CO_2 or pyrope-almandine + CO_2 are 50–150 °C lower than the calculated ones. The results obtained indicate that natural Mg,Fe-carbonates under subduction conditions at depths of ~ 90 km react with oxides in the temperature range 1000–1100 °C, ~ 190 km – 1150–1250 °C, and at depths of ~ 225 km – at 1400 °C.

The authors of the article thank A.G. Sokol for consultations on the methodology of high-pressure, high-temperature experiments with a hematite buffer container. This work was supported by the Russian Foundation for Basic Research (project No. 18-35-20016), and was performed on state assignment of the IGM SB RAS.

REFERENCES

Bataleva, Y.V., Palyanov, Y.N., Borzdov Y.M., Kupriyanov, I.N., Sokol, A.G., 2016. Synthesis of diamonds with mineral, fluid and melt inclusions. Lithos 265, 292–303.

Bataleva, Yu.V., Palyanov Yu.N., Sokol, A.G., Borzdov, Yu.M., Palyanova, G.A., 2012. Conditions for the origin of oxidized carbonate-silicate melts: implications for mantle metasomatism and diamond formation. Lithos 128–131, 113–125.

Berman, R.G., 1991. Thermobarometry using multiequilibrium calculations: a new technique with petrologic applications. Can. Mineral. 29, 833–855.

Boettcher, A.L., Mysen, B.O., Allen, J.C., 1973. Techniques for the control of water fugacity and oxygen fugacity for experimentation in solid-media high-pressure apparatus. J. Geophys. Res. 80 (26), 5898–5901.

Boulard, E., Gloter, A., Corgne, A., Antonangeli, D., Auzende, A.-L., Perrillat, J.-P., Guyot, F., Fiquet, G., 2011. New host for carbon in the deep Earth. Proceedings of the National Academy of Sciences of the USA, Vol. 10 (13), 5184–5187.

Boyd, F.R., Pearson, D.G., Nixon, P.H., Mertzman, S.A., 1993. Low-calcium garnet harzburgites from southern Africa: Their relation to craton structure and diamond crystallization. Contrib. Mineral. Petrol. 113 (3), 352–366.

Brenker, F.E., Vollmer, C., Vincze, L., Vekemans, B., Szymanski, A., Janssens, K., Szaloki, I., Nasdala, L., Joswig, W., Kaminsky, F., 2007. Carbonates from the lower part of transition zone or even the lower mantle. Earth Plan. Sci. Lett. 260, 1–9.

Bulanova, G.P., 1995. The formation of diamond. J. Geochim. Expl. 53, 2–23.

Bulanova, G.P., Pavlova, L.P., 1987. Magnesite peridotite mineral association in a diamond from the Mir pipe. Dokl. Akad. Nauk SSSR, 295 (6), 1452–1456.

Dasgupta, R., Hirschmann, M.M., 2010. The deep carbon cycle and melting in Earth's interior. Earth Plan. Sci. Lett. 298, 1–13.

Eggler, D.H., 1978. The effect of CO_2 upon partial melting of peridotite in the system Na_2O–CaO–Al_2O_3–MgO–SiO_2–CO_2 to 35 kbar, with an analysis of melting in a peridotite-H_2O–CO_2 system. Am. J. Sci. 278, 305–343.

Foley, S.F., 2010. A reappraisal of redox melting in the Earth's mantle as a function of tectonic setting and time. J. Petrol. 52 (7–8), 1363–1391.

Griffin, W.L., Fisher, N.I., Friedman, J., Ryan, C.G., O'Reilly, S.Y., 1999. Cr-pyrope garnets in the lithospheric mantle: I. Compositional systematics and relations to tectonic setting. J. Petrol. 40 (5), 679–704.

Gunn, S.C., Luth, R.W., 2006. Carbonate reduction by Fe-S-O melts at high pressure and high temperature. Am. Mineral. 91, 1110–1116.

Gurney, J.J., Harte, B., 1980. Chemical variations in upper mantle nodules from southern African kimberlites. Philosophical Transactions of the Royal Society of London, A297, 273–293.

Gurney, J.J., Jacob, W.R.O., Dawson, J.B., 1979. Megacrysts from the Monastery kimberlite pipe, South Africa, in: Boyd, F.R., Meyer, H.O.A. (Eds.), Kimberlites, Diatremes and Diamonds: Their Geology, Petrology and Geochemistry. American Geophysical Union: Washington. No. 1, pp. 222–243.

Gurney, J.J., Moore, R.O., Otter, M.L., Kirkley, M.B., Hops, J.J., McCandless, T.E., 1991. Southern African kimberlites and their xenoliths, in: Kampunzu, A.B., Lubala, R.T. (Eds.), Magmatism in Extensional Structural Settings. Springer: Berlin, pp. 495–536.

Gurney, J.J., Switzer, G.S., 1973. The discovery of garnets closely related to diamonds in the Finsch pipe, South Africa. Contrib. Mineral. Petrol. 39 (2), 103–116.

Harris, J.W., 1992. Diamond geology, in: Field, J.E. (Ed.), The Properties of Natural and Synthetic Diamond. Academic Press: London, pp. 345–393.

Harris, J.W., 1987. Recent physical, chemical and isotopic research of diamond, in: Nixon, P.H. (Ed.), Mantle Xenoliths. Wiley: Chichester, pp. 477–500.

Harte, B., Hawkesworth, C.J., 1989. Mantle domains and mantle xenoliths, in: Ross, J. (Ed.), Kimberlites and related rocks, Geological Society of Australia, Special Publication, No. 14, Vol. 2, pp. 649–686.

Holland, T. J. B., Powell, L., 1990. An enlarged and updated internally consistent thermodynamic dataset with uncertainties and correlations: K_2O–Na_2O–CaO–MgO–FeO–Fe_2O_3–Al_2O_3–TiO_2–SiO_2–C–H_2–O_2. J. Metamorph. Geol. 8, 89–124.

Izraeli, E.S., Harris, J.W., Navon, O., 2001. Brine inclusions in diamonds: a new upper mantle fluid. Earth Plan. Sci. Lett. 187, 1–10.

Jones, A., Genge, M., Carmody, L., 2013. Carbonate melts and carbonatites. Rev. Mineral. Geochem. 75 (1), 289–322.

Kadik, A.A., Lukanin, O.A., Kogarko, L.N., 1986. Degassing of the Upper Mantle During Melting [in Russian]. Nauka, Moscow.

Kalugina, A.D., Zedgenizov, D.A., 2019. Raman discrimination of garnet inclusions in Siberian diamonds. J. Raman Spectrosc. 1–7.

Kaminsky, F., Wirth, R., Schreiber, B., 2013. Carbonatitic inclusions in Deep Mantle diamond from Juina, Brazil: New minerals in the carbonate-halide association. Can. Mineral. 51, 669–688.

Kang, N., Schmidt, M.W., Poli, S., Connolly, J.A.D., Franzolin, E., 2016. Melting relations in the system $FeCO_3$–$MgCO_3$ and thermodynamic modelling of Fe–Mg carbonate melts. Contrib. Mineral. Petrol. 171 (8–9), Article 74.

Kang, N., Schmidt, M.W., Poli, S., Franzolin, E., Connolly, J.A.D., 2015. Melting of siderite to 20 GPa and thermodynamic properties of $FeCO_3$-melt. Chem. Geol. 400, 34–43.

Katsura, T., Ito, E., 1990. Melting and subsolidus relations in the Mg-SiO_3–$MgCO_3$ system at high pressures: implications to evolution of the Earth's atmosphere. Earth Plan. Sci. Lett. 99, 110–117.

Kennedy, C.S., Kennedy, G.C., 1976. The equilibrium boundary between graphite and diamond. J. Geoph. Res. 81, 2467–2470.

Knoche, R., Sweeney, R.J., Luth, R.W., 1999. Carbonation and decarbonation of eclogites: the role of garnet. Contrib. Mineral. Petrol. 135 (4), 332–339.

Kolesov, B., Geiger, C., 1998. Raman spectra of silicate garnets. Phys. Chem. Mineral. 25, 142–151.

Kopylova, M.G., Russell, J.K., Cookenboo, H., 1999. Petrology of peridotite and pyroxenite xenoliths from the Jericho kimberlite: Implications for the thermal state of the mantle beneath the Slave craton, northern Canada. J. Petrol. 40, 79–104.

Koziol, A.M., Newton, R.C., 1998. Experimental determination of the reaction: Magnesite + enstatite = forsterite + CO_2 in the ranges 6–25 kbar and 700–1100 °C. Am. Mineral. 83, 213–219.

Luth, R.W., 1999. Carbon and carbonates in mantle, in: Fei, Y., Bertka, M.C., Mysen, B.O. (Eds.), Mantle Petrology: Field Observation and High Pressure Experimentation: A Tribute to Francis R. (Joe) Boyd: The Geochemical Society, Special Publication, No. 6, pp. 297–316.

Luth, R.W., 1995. Experimental determination of the reaction dolomite + 2 coesite = diopside + 2 CO_2 to 6 GPa. Contrib. Mineral. Petrol. 122 (1–2), 152–158.

Luth, R.W., 1989. Natural versus experimental control of oxidation state: Effects on the composition and speciation of C-O-H fluids. Am. Mineral. 74, 50–57.

Martin, A.M., Hammouda, T., 2011. Role of iron and reducing conditions on the stability of dolomite + coesite between 4.25 and 6 GPa – a potential mechanism for diamond formation during subduction. Eur. J. Mineral. 23, 5–16.

Merlini, M., Crichton, W.A., Hanfland, M., Gemmi, M., Müller, H., Kupenko, I., Dubrovinsky, L., 2012. Structures of dolomite at ultrahigh pressure and their influence on the deep carbon cycle. Proc. Nat. Acad. of Sci. USA, 109 (34), 13509–13514.

Meyer, H.O.A., 1987. Inclusions in diamond, in: Nixon, P.H. (Ed.), Mantle Xenoliths. Wiley, Chichester, pp. 501–523.

Morlidge, M., Pawley, A., Droop, G., 2006. Double carbonate breakdown reactions at high pressures: An experimental study in the system CaO-MgO-FeO-MnO-CO_2. Contrib. Mineral. Petrol. 152 (3), 365–373.

Navon, O., Hutcheon, I.D., Rossman, G.R., Wasserburg, G.J., 1988. Mantle-derived fluids in diamond micro-inclusions. Nature 335, 784–789.

Newton, R.C., Sharp, W.E., 1975. Stability of forsterite + CO_2 and its bearing on the role of CO_2 in the mantle. Earth Planet. Sci. Lett. 26, 239–244.

Oganov, A.R., Hemley, R.J., Hazen, R.M., Jones, A.P., 2013. Structure, bonding and mineralogy of carbon at extreme conditions. Rev. Mineral. Geochem. 75 (1), 47–77.

Ogasawara, Y., Liou, J.G., Zhang, R.Y., 1997. Thermochemical calculation of logf_{O_2}-T-P stability relations of diamond-bearing assemblages in the model system CaO-MgO-SiO_2-CO_2-H_2O. Geologiya i Geofizika (Russian Geology and Geophysics), 38 (2), 546–557 (587–598).

Pal'yanov, Y.N., Sokol, A.G., Khokhryakov, A.F., Pal'yanova, G.A., Borzdov, Y.M., Sobolev, N.V., 2000. Diamond and graphite crystallization in COH fluid at PT parameters of the natural diamond formation. Dokl. Earth Sci. 375, 1395–1398.

Pal'yanov, Yu.N., Sokol, A.G., Tomilenko, A.A., Sobolev, N.V., 2005. Conditions of diamond formation through carbonate-silicate interaction. Eur. J. Mineral. 17 (2), 207–214.

Palyanov, Y.N., Bataleva, Y.V., Sokol, A.G., Borzdov, Y.M., Kupriyanov, I.N., Reutsky, V.N., Sobolev, N.V., 2013. Mantle–slab interaction and redox mechanism of diamond formation. Proceedings of the National Academy of Sciences of the USA, Vol. 110 (51), 20408–20413.

Palyanov, Yu.N., Borzdov, Yu.M., Bataleva, Yu.V., Sokol, A.G., Palyanova, G.A., Kupriyanov, I.N., 2007. Reducing role of sulfides and diamond formation in the Earth's mantle. Earth Plan. Sci. Lett. 260 (1–2), 242–256.

Palyanov, Yu.N., Borzdov, Yu.M., Khokhryakov, A.F., Kupriyanov, I.N., Sokol, A.G., 2010. Effect of nitrogen impurity on diamond crystal growth processes. Cryst. Growth Des. 10, 3169–3175.

Palyanov, Yu.N., Sokol, A.G., 2009. The effect of composition of mantle fluids/melts on diamond formation processes. Lithos 112S, 690–700.

Palyanov, Y.N., Kupriyanov, I.N., Khokhryakov, A.F., Borzdov, Y.M., 2017. High-pressure crystallization and properties of diamond from magnesium-based catalysts. CrystEngComm, 19 (31), 4459–4475.

Pearson, D.G., Canil, D., Shirey, S.B., 2003. Mantle Samples Included in Volcanic Rocks: Xenoliths and Diamonds, in: Treatise on Geochemistry. Elsevier, Amsterdam, Vol. 2, pp. 171–275.

Perchuk, A.L., Serdyuk, A.A., Zinovieva, N.G., 2019. Subduction sediment–lherzolite interaction at 2.9 GPa: Effects of metasomatism and partial melting. Petrology 27 (5), 467–488.

Plank, T., Manning, C.E., 2019. Subducting carbon. Nature 574, 343–352.

Pokhilenko, N.P., Sobolev, N.V., Boyd, F.R., Pearson, D.G., Shimizu, N., 1993. Megacrystalline pyrope peridotites in the lithosphere of the Siberian platform: Mineralogy, geochemical peculiarities and the problem of their origin. Geologiya i Geofizika (Russian Geology and Geophysics) 34 (1), 71–84 (56–67).

Robie, R.A., Hemingway, B.S., Fischer, J.R., 1978. Geological Survey Bulletin 1452. United States Government, Printing Office, Washington.

Schrauder, M., Navon, O., 1994. Hydrous and carbonatitic mantle fluids in fibrous diamonds from Jwaneng, Botswana. Geoch. Cosmoch. Acta 58, 761–771.

Shatskiy, A., Podborodnikov, I.V., Arefiev, A.V., Minin, D.A., Chanyshev, A.D., Litasov, K.D., 2018. Revision of the $CaCO_3$–$MgCO_3$ phase diagram at 3 and 6 Gpa. Am. Mineral. 103, 441–452.

Shatskiy, A.F., Litasov, K.D., Palyanov, Y.N., 2015. Phase relations in carbonate systems at pressures and temperatures of lithospheric mantle: review of experimental data. Russian Geology and Geophysics (Geologiya i Geofizika) 56 (1–2), 113–142 (149–187).

Shirey, S.B., Cartigny P., Frost D.G., Keshav S., Nestola F., Nimis P., Pearson D.G., Sobolev N.V., Walter M.J. Diamonds and the geology of mantle carbon. Rev. Mineral. Geochem. 75, 355–421.

Sobolev, N.V., 1970. Eclogites and pyrope peridotites from the kimberlites of Yakutia. Phys. Earth Plan. Inter. 3, 398–404.

Sobolev, N.V., 1977. The Deep-Seated Inclusions in Kimberlites and the Problem of the Composition of the Upper Mantle. American Geophysics Union, Washington.

Sobolev, N.V., Kaminsky, F.V., Griffin, W.L., Yefimova, E.S., Win, T.T., Ryan, C.G., Botkunov, A.I., 1997. Mineral inclusions in diamonds from the Sputnik kimberlite pipe, Yakutia. Lithos 39, 135–157.

Sobolev, N.V., Lavren'tev, Yu.G., Pospelova, L.N., Sobolev, E.V., 1969. Chrome pyropes from Yakutian diamonds. Dokl. Akad. Nauk, 1969, 189 (1), 162–165.

Sobolev, N.V., Lavrent'yev, Y.G., Pokhilenko, N.P., Usova, L.V., 1973. Chrome-rich garnets from the kimberlites of Yakutia and their paragenesis. Contrib. Mineral. Petrol. 40 (1), 39–52.

Sobolev, N.V., Logvinova, A.M., Tomilenko, A.A., Wirth, R., Bul'bak, T.A., Luk'yanova, L.I., Fedorova, E.N., Reutsky, V.N., Efimova, E.S., 2019. Mineral and fluid inclusions in diamonds from the Urals placers, Russia: Evidence for solid molecular N_2 and hydrocarbons in fluid inclusions. Geoch. Cosmochim. Acta 266, 197–219.

Sobolev, N.V., Shatsky, V.S., Zedgenizov, D.A., Ragozin, A.L., Reutsky, V.N., 2016. Polycrystalline diamond aggregates from the Mir kimberlite pipe, Yakutia: Evidence for mantle metasomatism. Lithos 265, 257–266.

Sobolev, N.V., Snyder, G.A., Taylor, L.A., Keller, R.A., Yefimova, E.S., Sobolev, V.N., Shimizu, N., 1998. Extreme chemical diversity in the mantle during eclogitic diamond formation: Evidence from 35 garnet and 5 pyroxene inclusions in single diamond. Intern. Geol. Rev. 40, 567–578.

Sobolev, V.S., Sobolev, N.V., 1980 New evidence of the submergence of eclogitized rocks of the Earth's crust at great depths. Dokl. Akad. Nauk SSSR 250, 683–685.

Sokol, A.G., Borzdov, Y.M., Palyanov, Y.N., Khokhryakov, A.F., 2015. High-temperature calibration of a multi-anvil high pressure apparatus. High Press. Res. 35 (2), 139–147.

Sokol, A.G., Khokhryakov, A.F., Palyanov, Yu.N., 2015. Composition of primary kimberlite magma: constraints from melting and diamond dissolution experiments. Contrib. Mineral. Petrol. 170 (3), Article 26.

Stachel, T., Harris, J.W., Brey, G.P., 1998. Rare and unusual mineral inclusions in diamonds from Mwadui, Tanzania. Contrib. Mineral. Petrol. 132 (1), 34–47.

Stagno, V., 2019. Carbon, carbides, carbonates and carbonatitic melts in the Earth's interior. J. Geol. Soci. 176, 375–387.

Tao, R., Fei, Y., Zhang, L., 2013. Experimental determination of siderite stability at high pressure. Am. Mineral. 98, 1565–1572.

Wang, A., Pasteris, J.D., Meyer, H.O.A., DeleDuboi, M.L., 1996. Magnesite-bearing inclusion assemblage in natural diamond. Earth Plan. Sci. Lett. 141 (1–4), 293–306.

Wendlandt, R.F., Huebner, S.J., Harrison, W.J., 1982. The redox potential of boron nitride and implications for its use as a crucible material in experimental petrology. Am. Mineral. 67 (1–2), 170–174.

Wyllie, P.J., 1979. Magmas and volatile components. Am. Mineral. 64, 469–500.

Wyllie, P.J., Huang, W.-L., Otto, J., Byrnes, A.P., 1983. Carbonation of peridotites and decarbonation of siliceous dolomites represented in the system CaO-MgO-SiO_2-CO_2 to 30 kbar. Tectonophysics 100 (1–3), 359–388.

Editorial responsibility: N.V. Sobolev